Role of low-pass filtering in the process of attractor reconstruction from experimental chaotic time series

William F. Lawkins, C. Stewart Daw, Darryl J. Downing, and Ned E. Clapp, Jr.
Oak Ridge National Laboratory, P.O. Box 2008, Oak Ridge, Tennessee 37831-6367
(Received 24 June 1992; revised manuscript received 9 November 1992)

We discuss issues concerning the reconstruction of attractors from experimental chaotic time-series data using Takens's method of delays [in *Proceedings of the Warwick Symposium, 1981,* edited by D. A. Rand and L. S. Young (Springer, New York, 1981)]. The focus of this paper is on the selection of appropriate lag-time and embedding-dimension values with an emphasis on the relationship between those parameters and data-measurement considerations. We are particularly interested in the effect that low-pass filtering has on the appearance and measured properties of reconstructed attractors. Empirical results are presented using data measured from a laboratory fluidized bed and from data generated by integrating the Lorenz [J. Atmospheric Sci. **20**, 130 (1963)] and Franceschini [Physica **6D**, 285 (1983)] models of chaotic dynamic systems.

PACS number(s): 47.20.Ky

I. INTRODUCTION

The modern point of view, borrowed from Poincaré and extended more recently by other researchers, is that nonlinear dynamical systems are, in general, represented by attractors in state space. The characterization or analysis of such a nonlinear dynamical process is, in turn, largely equivalent to studying (a) the geometric structure of the attractor, (b) the flow properties of trajectories on the attractor, and (c) the relationships between the geometric structure and flow properties. In this paper we address issues concerning attractor reconstruction from time series data using Takens's method of delays [1]. We are particularly interested in questions about the analysis of time-series measurements of real engineering systems and how background processes, including noise, can affect the attractor reconstruction results. The role played by low-pass filtering in the data-analysis process is the theme of this paper. That role is examined from two standpoints: First, we consider the use of low-pass filtering to compensate for background information and noise in the data, and second, we consider the use of low-pass filtering as a diagnostic tool for examining the structure of the attractor. In a companion paper, we will address the related problem of analyzing flow on the reconstructed attractor. Together, these papers give details and expand on results reported in a Rapid Communication [2].

The attractor-reconstruction examples given in this paper derive primarily from experimental time-series data measured from a complex gas-solids flow. In order to relate what we do to that reported by other researchers, we also use time series generated from the Lorenz [3] and Franceschini [4] model systems of ordinary differential equations. Another reason for also using model data is to explore the extent to which lessons learned using it can be carried over to the context of experimental data.

The approach we investigate in this paper for implementing Takens's method for attractor reconstruction follows the direction described by Broomhead and King [5]. In their approach, Broomhead and King use the spectral density and autocorrelation of a random variable, here represented by a measured time series, together with the singular values of the so-called trajectory matrix to establish conditions for choosing values of the lag-time and embedding-dimension parameters. Using the data described above, we test the guidelines posed by Broomhead and King for choosing those parameter values. In particular, we look at how those parameter values are affected by moving the low-pass filter-cutoff point.

As stated above, we are especially interested in applications using experimental data representative of engineering systems and realistic measurement conditions. Under such conditions, the environment in which a measurement is made is likely to make a nontrivial contribution to the frequency content of the measured variable and, thus, affect the attractor-reconstruction process. The primary objective of the work presented here is to evaluate whether the guidelines posed by Broomhead and King for choosing the lag-time and embedding-dimension values have to be modified due to the presence of background processes and noise. In addition, we study the effect on the reconstruction process of varying the filter-cutoff point over a range of values for which the energy of the process of interest clearly dominates that of the background. This is done for two reasons. First, we want to see if information about the geometric structure of the attractor is well mixed among the frequencies. Second, we want to determine whether additional information about the process can be gained by, in a sense, successively stripping away increasing amounts of detail from the measured data by filtering. For example, we might expect to gain a better view of the large-scale structure of the reconstructed attractor this way.

The relationship between the attractor-reconstruction process and the three parameters lag time, embedding dimension, and filter-cutoff point is studied the following way: First, for a given reconstructed attractor, the correlation integral [6] is calculated and used as a quantitative

observable of that attractor. Second, the singular values of the trajectory matrix discussed by Broomhead and King [5] are analyzed in terms of filter-cutoff frequency and "window" length. Then, the effect of changing parameter values on the singular values is related to observed effects on the correlation integral.

Before proceeding, we want to acknowledge two areas of research previously reported in the literature that are important to be aware of because they have bearing on the material presented here. First, filtering is part of all real data measurement processes and, so, it is of very practical importance to know how the act of filtering impacts the reconstruction process, which we understand to include all information embodied in the reconstructed attractor about the process of interest. Badii *et al.* [7], followed by Mitschhe, Moller, and Lange [8], have contributed toward developing an understanding about the presence of low-pass filters on measures of chaotic structure as represented by reconstructed attractors. More recently, Broomhead, Huke, and Muldoon [9] have investigated the same topic, and, in particular, have given a heuristic explanation for the observations of the aforementioned researchers. The scope of the present paper does not permit us to analyze points made by those researchers relative to the fluidized-bed analyses presented here, but we will outline the conclusions reached by those researchers and describe how the fluidized-bed results do, or do not, reflect those conclusions. We plan to examine this issue quantitatively in a future paper.

Fraser and Swinney [10] and Fraser [11] have proposed and studied another means than the Broomhead and King approach for implementing Takens's method of delays. The difference in approaches for selecting lag-time and embedding-dimension values owes largely to the difference in the correlation and mutual information measures of independence between two random variables (see Fraser [11] for a comparative description of the difference in those measures). It should be noted that Fraser [11] is critical of the Broomhead and King technique. In this paper we make no attempt at comparing the two methods or at arguing the relative merit of one over the other.

The remainder of this paper is organized as follows. In Sec. II we describe the generation of our experimental and numerical time series, discuss the low-pass filter we use, and present spectral density functions for the data. In this section we also review work by other researchers concerning filters. In Sec. III, we present the results of our studies. For completeness, we also review the Broomhead and King approach for selecting lag-time and embedding-dimension values and display the form of the definition of correlation integral used to make calculations. Finally, in Sec. IV we summarize our findings.

II. TIME-SERIES DATA

In this section we discuss the time-series measurements. We also describe the filtering technique used to process the data subsequent to measurement. Spectral density curves for the data are displayed. We conclude this section with a review of the work concerning filters by Badii *et al.* [7], Mitschhe, Moller, and Lange [8], and Broomhead, Huke, and Muldoon [9].

A. Experimental fluidized-bed measurements

Fluidized beds are generic processing devices used widely in the chemical and petroleum industries to generate intimate physical contact between fluids and particulate solids. The particles are typically contained in a vertically oriented vessel and the fluid enters from the bottom and exits from the top. The upward drag of the fluid balances counteracting gravity, causing the particles to whirl about in complex patterns that depend on the influx rate of the fluid.

In the experiments used to generate data for this paper, the fluidized bed consisted of a vertical 10.2-cm-diam pipe filled to a static depth of 11 cm with granular corn, or maize, particles approximately 5 mm in diameter. Corn was used for this experiment because of a particular interest in the dynamical behavior of relatively large, irregularly shaped particles. Air flows into the pipe through a multiple-orifice distributor that produces a sufficient pressure drop to decouple the fluidization dynamics from the air-supply system. After passing through the particles, the air exists the pipe directly into the atmosphere. The overall pressure drop between the bottom of the bed just above the air distributor and the atmosphere was measured with a fast-response piezoelectric pressure transducer. The time series used in this paper correspond to the fluctuations in that pressure drop.

Data-acquisition rates were typically 500 samples/sec and the records used for this paper were typically 2×10^4 points. Before digitization and storage, pressure transducer signals were amplified to maximize resolution of the signal fluctuations. The signals were then filtered through high- and low-pass analog filters having a 24 dB per octave (80 dB per decade) rolloff. High-pass filtering was done at 0.1 Hz to eliminate dc and establish a frequency minimum (maximum period) for subsequent analysis. Low-pass filtering (anti-aliasing filtering) was done at 40 Hz to establish a frequency maximum (minimum period) and to remove frequencies that could interfere with the sampling process to produce low-frequency artifacts (i.e., Nyquist folding frequencies [12]). The low-pass frequency (40 Hz) was used, in part, to insure the removal of the 60-Hz line frequency.

In accord with good experimental practice, we made reasonable efforts to shield the pressure transducer from outside vibration and the data-acquisition equipment from external electrical fields. We deliberately did not make extraordinary measures to shield the transducer, however, in order to produce "realistically noisy" data. To obtain a direct estimate of the inherent noise in the measurement system, we also captured data for a null condition; i.e., a completely stationary bed through which no air was flowing.

Figure 1 depicts portions of the as-measured time series for the superficial (i.e., open-tube) air velocities 2.4 and 5.7 m/s, respectively. Corresponding open-tube Reynolds numbers for those flows are 1.35×10^4 and 3.77×10^4. The two positive air flows produce distinct turbulence patterns. The pattern at 2.4 m/s is typically designated as "slugging" and is characterized by large pressure swings produced by gas pockets ("bubbles") that move up alternately with clumps of solids. During slug-

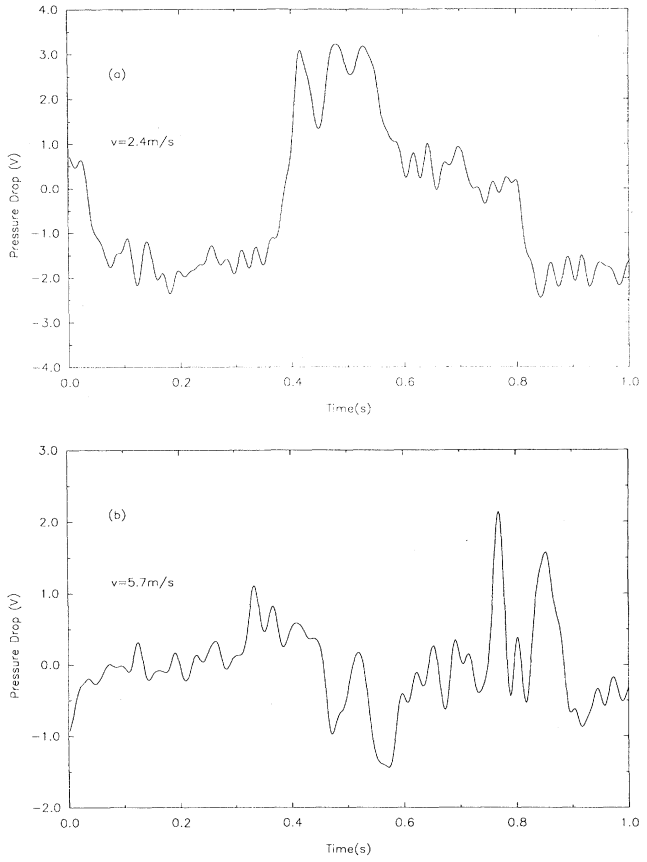

FIG. 1. Fluidized-bed time series: (a) $v=2.4$ m/s; (b) $v=5.7$ m/s.

ging, the gas pockets become large enough to fill the tube cross section. At 5.7 m/s the pressure swings are reduced, well-defined bubbles are absent, and the clumps of solids are replaced by "strands" that appear to constantly break and reform.

Figure 2 displays the power spectrums for the two positive air flow time-series measurements and for the null-condition measurement. Note that the power in the 2.4-m/s data is concentrated in a dominant peak near 2 Hz and a lesser peak at approximately 4 Hz. These two peaks reflect the physical phenomenon of slugging, which, as described above, means the solids tend to move collectively as a large slug and, likewise, the gas as a large void. The power in the 5.7-m/s data is much more dispersed, reflecting the broader range of flow velocities that simultaneously occur in this state. Beds operating in the latter regime are said to exhibit "fast fluidization" and are characterized by small and highly mixed solid-gas regions. In a slugging state, large pockets of gas pass through the bed without making very much surface area contact with solids, which is in contrast with a fast fluidization state. For that reason, the fast fluidization state is in general more desirable than the slugging state from an applications standpoint. These two data sets are used in this paper because they represent very different physical regimes in a gas fluidized-bed process.

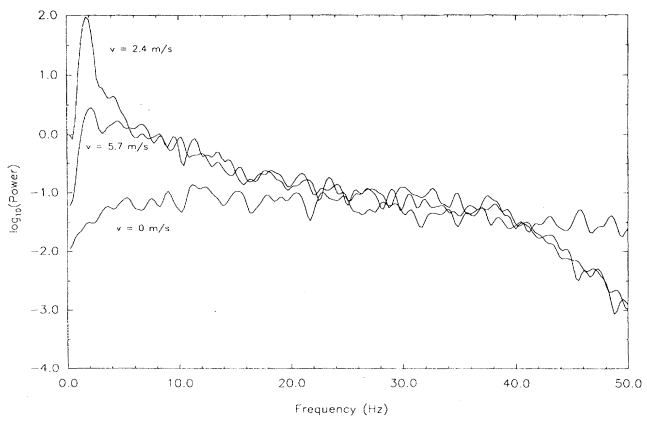

FIG. 2. Fluidized-bed spectral density functions.

B. Ordinary differential-equation model data

We use the Lorenz [3] and Franceschini [4] model systems of ordinary differential equations to generate model data. The Lorenz model is very well known, and, in particular, Broomhead and King use it for an example of the application of their reconstruction method [5]. The Lorenz equations are displayed in the Broomhead and King paper and the notation we use here coincides with that used by those researchers. Mimicking Broomhead and King, the parameter values we use for the Lorenz model are $\sigma=10$, $b=\frac{8}{3}$, and $r=28$, and we use the x component of the system equations to generate time-series data. The sample time we use for the Lorenz data is again the same one used by Broomhead and King, namely, $t_s=0.003$.

The Franceschini model is a system of seven ordinary differential equations that approximates incompressible fluid flow on the surface of a two-dimensional torus [4]. Franceschini reports that the model exhibits a series of bifurcations as a Reynolds number parameter, denoted R, is varied over the range 226.0–299.0 and that the system first loses its stability to a strange attractor at approximately $R=299.25$. The Franceschini-model time-series data used in this paper is that for $R=310.0$, a value for which chaotic behavior is well developed. The recorded time-series variable is the first component of the Franceschini model (see Eq. (4) in the Franceschini paper [4]).

A variable-order and variable-time-step Adams integrator, SUBROUTINE DEABM, from the well-known mathematical software library SLATEC is used to integrate the Lorenz- and Franceschini-model equations [13,14]. For such an integrator, the user supplies the output times, which in this case corresponds to the preselected sampling rate, while the integrator is free to vary the integration time step a well as order in keeping with user-supplied error criteria.

Because we are using spectral density curves of discretely sampled data, regardless of whether the "system" is real, like a fluidized bed, or a model system of ordinary differential equations, Nyquist folding has to be taken into account. The discretely sampled data, for ex-

ample, the first component of the Franceschini model, is accurate to the precision specified by the user to the numerical integrator, but a spectral density analysis of that data will reflect the Nyquist-folding effect. To mitigate that effect, we integrate in parallel with the model equations a four-stage, linear filter based on the first-order equation

$$\frac{1}{\omega}\frac{dy}{dt}+y=x \ , \tag{2.1}$$

where x is input, y is output, $\omega=2\pi f$, $f=1/(2t_s)$ is the Nyquist frequency, and t_s^{-1} is the sampling rate. For instance, referring to the Franceschini model, the first component of the model system is input to the first stage of the four-stage filter. The output from the fourth stage of the filter is the measured time series of the model system.

We point out that the accuracy criteria specified by the user to the numerical integrator establishes a noise floor in the measured data as represented, for example, by a spectral density analysis. If that data is subsequently filtered again, such as we describe below, that floor will be reduced until ultimately the floor associated with the arithmetic precision of the computer being used is reached. That does not mean the more highly filtered data is more precise than the original set. Clearly, the accuracy of the data for frequencies less than the filter-cutoff point is exactly the same as that of the original measured set.

Figure 3 shows filtered and unfiltered spectral density curves for the Lorenz and Franceschini models. For the Franceschini model, Fig. 3(a) shows spectral density curves for the filtered and unfiltered time series corresponding to the sampling rate $t_s^{-1}=10^3$ Hz, and Figs. 3(b) and 3(c) display spectral density curves for the filtered and unfiltered time series corresponding to the sampling rate $t_s^{-1}=6$ Hz. The power spectrums displayed in Fig. 3(a) imply, first, the sampling frequency used in that case is sufficiently high to resolve all the meaningful frequencies in the system, and second, that the information in the filtered and unfiltered variables is the same. In the second case, however, the sampling rate does not resolve all meaningful frequencies in the system, and, consequently, there is a difference in the information content of the filtered and unfiltered variables. A comparison of Figs. 3(b) and 3(c) illustrates the result of folding, whereby information in frequencies greater than the Nyquist frequency is folded back into the frequency range bounded above by the Nyquist frequency. Turning to the Lorenz model, Fig. 3(d) displays the spectral density functions for the filtered and unfiltered discrete variable. Clearly, the significant frequencies are resolved by the chosen sampling rate ($t_s^{-1}=3.33\times10^2$ Hz).

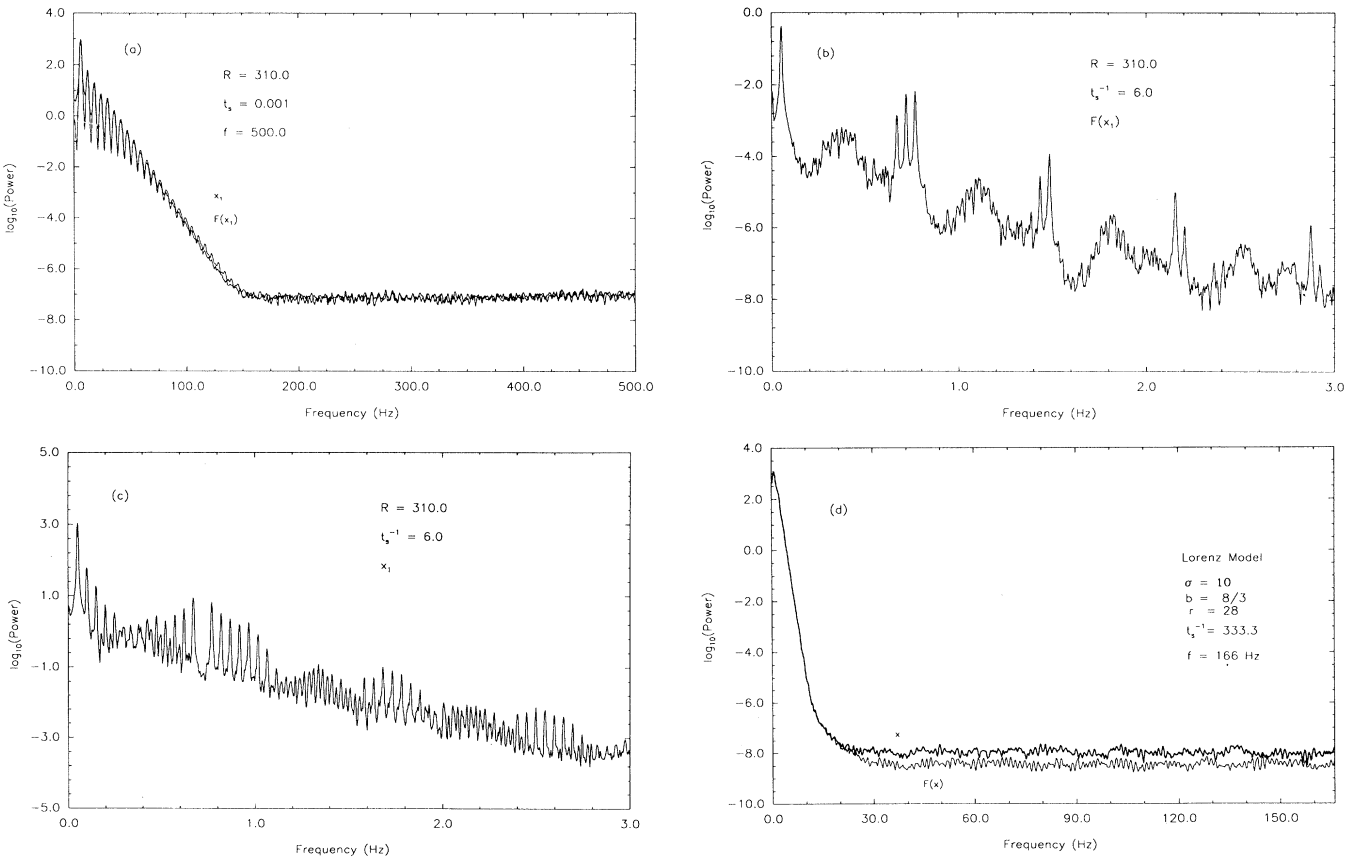

FIG. 3. Model spectral density functions: (a) Franceschini model, filtered and unfiltered data, $t_s=0.001$; (b) Franceschini model, filtered data, $t_s^{-1}=6.0$; (c) Franceschini model, unfiltered data, $t_s^{-1}=6.0$; (d) Lorenz model, filtered and unfiltered data, $t_s=0.003$.

C. Digital low-pass filtering

The low-pass filter described by Eq. (2.1) can be analytically integrated. Doing so leads to the digital filter

$$y_{i+1}=y_i\exp(-\omega t_s)+x_i[1-\exp(-\omega t_s)]\ , \qquad (2.2)$$

where y_i is the output value at time t_i, x_i is the input value at time t_i, $\omega=2\pi f$, f is the characteristic filter-cutoff frequency, and $t_s=t_{i+1}-t_i$. Low-pass filtering of the time-series data, both experimental and model, at frequencies below the Nyquist frequency is accomplished using this digital filter. Equation (2.2) is referred to in control theory as a first-order lag (or first-order infinite-impulse-response filter) and is frequency used to simulate the behavior of measurement components [15]. We repeat the filtering four times, which is to say the output of the first stage is input to the second and so forth, to give the digital filter a similar frequency rolloff characteristic to that of the analog filter. The resulting effect is equivalent to a fourth-order lag.

The characteristic response time of the filter is $1/2\pi f$, where f is the low-pass frequency. In effect, the filter can be used to simulate changes in the responsiveness, or inertia, of the measurement system by adjusting the value of f, where lower values of f result in deceased responsiveness. Variations in the signal occurring at time scales smaller than $1/2\pi f$ are effectively smoothed while variations occurring at time scales longer than $1/2\pi f$ remain unaffected.

Recall that Fig. 2 illustrates spectral densities for the fluidized-bed measured data. Figures 4(a) and 4(b) show spectral densities for the fluidized-bed data successively filtered using filter-cutoff values $f=24$, 8, 4, and 2 Hz. The background is not displayed in Figs. 4(a), and 4(b). However, if we displayed a plot of the power spectrums for the two experimental time series filtered, say, at $f=24$ Hz and added to that plot the power spectrum of the measured background also filtered at $f=24$ Hz, the plot would show the powers of experimental processes both dominate that for the background over the full range of frequencies. Figure 4(c) displays spectral density curves for the Lorenz time-series data filtered using the cutoff values $f=166$, 6, 3, and 1.5 Hz. Finally, Fig. 4(d) shows spectral density curves for the Franceschini-model data filtered using the cutoff values $f=250$, 50, and 30 Hz.

D. Previous research concerning the effect of filtering on estimates of dimension

One point of view that can be adopted regarding the act of making a quantitative measurement of some ob-

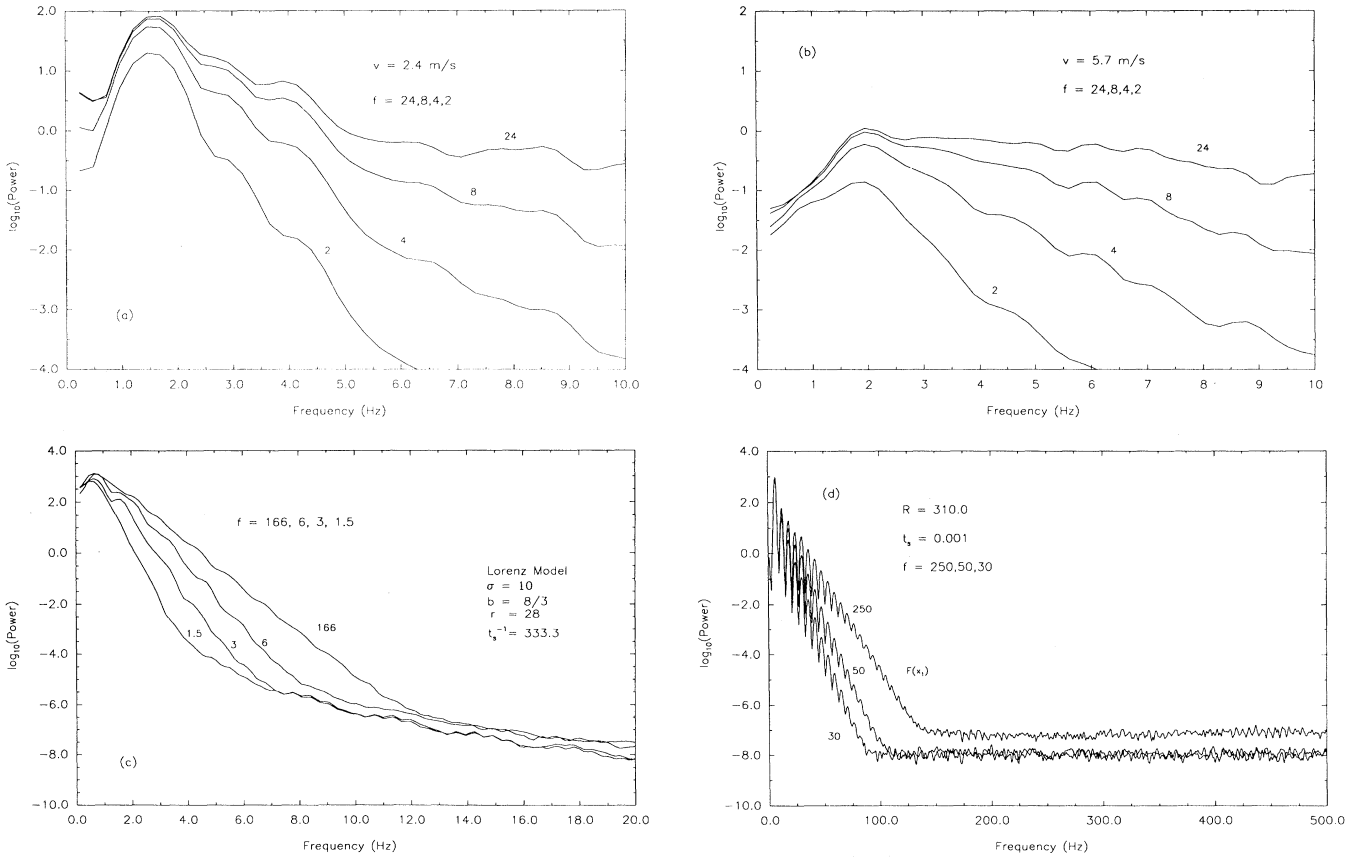

FIG. 4. Spectral density functions for filtered data: (a) Fluidized-bed data, $v=2.4$ m/s; (b) fluidized-bed data, $v=5.7$ m/s; (c) Lorenz data; (d) Franceschini data.

servable associated with a physical process, for example, a fluidized bed, is that the process actually observed is the coupled system corresponding to the physical process and the instrument for making the measurement. Consider, for example, the process represented by coupling the Lorenz equations with an instrument represented by the low-pass linear filter Eq. (2.1). Referring to the spectral density curves for the Lorenz process, Fig. 3(d), if the filter cutoff frequency is set greater than approximately 20 Hz so that frequencies with energy above the noise floor are resolved, then the filtered and unfiltered observables will contain the same dynamical information. Again referring to Fig. 3(d), if, on the other hand, the filter-cutoff point was set at, say, 1 Hz, then the process corresponding to the Lorenz equations coupled with the filter and represented by the filtered observable would be significantly different than that of the Lorenz equations alone. Information in the observable for frequencies greater than the cutoff frequency, but less than the frequency where the noise floor is reached, reflects the filter and not the process being observed.

The effect of observing a process using a low-pass filtered observable has been considered by Badii *et al.* [7]. Subsequently, Mitschhe, Moller, and Lange [8] tested the idea described by Badii, *et al.* [7] using experimental as well as model data. The essence of the idea can be described using the example described above, namely, the model process consisting of the Lorenz model coupled with the low-pass-filter model Eq. (2.1). Adding the low-pass filter Eq. (2.1) to the system of Lorenz equations increases the number of Lyapunov exponents from three to four for the coupled system. As long as the cutoff frequency of the low-pass filter is sufficiently high, the new stable Lyaponov exponent in the coupled system will be less than the stable Lyaponov exponent in the Lorenz system and, therefore, the Lyaponov dimension of the coupled system will be the same as that of the Lorenz process alone (see Eq. (2) in Ref. [7]). If, on the other hand, the filter-cutoff frequency is reduced to the point that the new stable Lyaponov exponent is greater than the stable Lyaponov exponent of the Lorenz system, than the Lyaponov dimension of the coupled process will be greater than that of the Lorenz process.

Broomhead, Huke, and Muldoon [9] have investigated, first, the effect of nonrecursive linear filters on the reconstruction process and, second, have used that result to heuristically explain observations concerning estimates of dimension made by Badii *et al.* [7] and Mitschhe, Moller, and Lange [8]. Consider the linear filter

$$y_i=\sum_{j=1}^{n_1} a_j y_{i-j}+\sum_{j=0}^{n_2-1} b_j x_{i-j} \ , \tag{2.3}$$

where x is input and y is output. If the right-hand side of this expression depends only on x, that is, if all the coefficients $a_j=0$, then the filter is nonrecursive. Otherwise, the filter is recursive. Note that the filter defined by Eq. (2.2) has the form

$$y_{i+1}=ay_i+bx_i \ , \tag{2.4}$$

where $0<a<1$ and $b=1-a$. This filter is recursive. According to Broomhead, Huke, and Muldoon [9], dimension is invariant in the case that the output of a finite-order nonrecursive filter is used for the attractor-reconstruction process. They go on to point out that a recursive filter can be represented as the limit of a sequence of nonrecursive filters. Consider the recursive filter Eq. (2.4). Suppose we replace y_i on the right-hand side by the expression obtained from Eq. (2.4) by replacing $i+1$ by i, which produces an expression with y_{i-1} appearing on the right-hand side. Next, replace y_{i-1} by the expression obtained from Eq. (2.4) by replacing $i+1$ by $i-1$, and so forth. Repeating this recursive process n times produces

$$y_{i+1}=a^n y_{i-n}+\sum_{j=0}^{n-1} a^j b x_{i-j} \ . \tag{2.5}$$

As $0<a<1$, for n sufficiently large, y_{i+1} is approximated by the nonrecursive expression

$$y_{i+1}\approx\sum_{j=0}^{n-1} a^j b x_{i-j} \ . \tag{2.6}$$

Referring to the recursive filter defined by Eq. (2.2), the filter constant a is defined in terms of the filter-cutoff frequency f and the sampling rate t_s^{-1} by

$$a=\exp(-2\pi f t_s) \ . \tag{2.7}$$

Assume the sampling rate is fixed. Then, the magnitude of a^n for a given value of n is determined by ft_s. That is, for a given magnitude, the lower the cutoff frequency f, the higher the order n such that a^n is that magnitude. If, in particular, we are working in finite precision arithmetic, then, to that precision, the recursive filter Eq. (2.4) is equivalent to the nonrecursive filter Eq. (2.6) for the value n such that a^n is the magnitude of that precision. Broomhead, Huke, and Muldoon argue heuristically that, if the order n is large, then a calculation of dimension using limited amounts of data can result in overestimates of dimension. We will return to this statement in the summary section and describe the reasoning behind it using ideas developed in this paper.

Recall that we use a four-stage filter, where each stage has the form Eq. (2.4). Leaving aside details, the effect of using a four-stage filter is approximately equivalent to using a single stage with a as defined above Eq. (2.7) replaced by a^4.

III. ATTRACTOR RECONSTRUCTION RESULTS

In this section we study the relationship between the attractor-reconstruction process and the three parameters (i) lag time, (ii) embedding dimension, and (iii) filter-cutoff frequency. We begin with a brief review of the Broomhead and King approach for implementing Takens's reconstruction procedure and of the definition of correlation integral.

A. Reconstruction method and correlation integral definition

According to Takens's method of delays [1], the system attractor is reconstructed from time-series measurements

by forming a trajectory in E^n, Euclidean n-dimensional space, using the relationship

$$p(i)=(\theta(i),\theta(i+k),\theta(i+2k),\ldots,\theta(i+(n-1)k))^T , \tag{3.1}$$

where $p(i)$ is the embedded point in E^n, $\theta(i)$ is the ith measurement, k is an integral lag time, and T denotes matrix transpose. The ith row of the trajectory matrix P is $p(i)^T$. In the subsequent discussion, we refer to the total time spanned by the trajectory vector,

$$t_w=(n-1)kt_s , \tag{3.2}$$

where t_s^{-1} is the data-measurement rate, as the "embedding window." As pointed out in Sec. I, the biggest problem associated with implementing this embedding procedure is selecting "correct" values for k and n.

Broomhead and King [5] propose that the length of the embedding window should be determined by the highest frequency for which significant power exists in the power spectrum of the measured variable θ. Referring to the spectral density function for the measured Lorenz data, Fig. 3(d), one possibility is to identify that time scale with the frequency where the power spectrum level reaches the noise floor, which is $t_n^{-1}\approx 20$ Hz. Once t_n is established, according to Broomhead and King n and k should be selected to satisfy the condition

$$t_w\approx t_n . \tag{3.3}$$

To proceed, Broomhead and King construct the trajectory covariance matrix

$$\Xi=1/NP^TP=1/N\sum_{i=1}^{N}p_ip_i^T , \tag{3.4}$$

where N is the total number of trajectory points, and analyze the eigenvalues and eigenvectors of that matrix. Those eigenvalues are also identified as the singular values of the trajectory matrix P. Assuming t_n is known and using the condition Eq. (3.3), a series of pairs (k,n) is chosen with n increasing and the series of resulting eigenvalues of $\Xi(k,n)$ is calculated. According to Broomhead and King, appropriate values for (k,n) are selected by applying the criterion that the significant eigenvalues of $\Xi(k,n)$ are converged. The remaining eigenvalues serve to establish a quantitative measure of the noise floor in the data.

Having selected k and n values, Broomhead and King go on to transform the trajectory Eq. (3.1) to a new set of Cartesian coordinates for E^n determined by the eigenvectors of the trajectory covariance matrix Ξ. The eigenvectors of Ξ, denoted for the moment by v_j, are orthogonal. Normalizing the eigenvectors by the condition $v_j^Tv_j=1$, the coordinates of the transformed trajectory are simply $p_i^Tv_j$, $j=1,\ldots,n$. It is important to remember that this transformation is geometry preserving and absolutely no distortion in the reconstructed attractor is introduced in the process. Measures of the dispersion of the attractor about the transformed coordinate axes, called the principal axes, are given by the eigenvalues of Ξ, which are equivalent to standard deviations in the principal directions. The components corresponding to purely noisy eigenvalues only result in adding a "skin thickness" to the attractor in those coordinate directions.

We want to make three observations about the reconstruction process described thus far. First, referring to Eq. (3.3), the first step in the Broomhead and King approach is to establish the window length t_w. In order to do this, it is implicitly assumed, first, that the data have been measured at a sufficiently high rate to resolve all meaningful dynamics of the system and, second, that there is a clear and unambiguous frequency t_n^{-1} bounding the range of information from that of noise, such as is illustrated in the Lorenz data [Fig. 3(d)]. Second, in the Broomhead and King approach, k is decreased as n is increased while maintaining the condition $t_w\approx t_n$ until, in effect, the significant eigenvalues of the covariance matrix Ξ, Eq. (3.4), are resolved (see Fig. 7 in Broomhead and King [5]). The resulting lag-time value k is then used by Broomhead and King to establish the "right" sampling rate, namely, kt_s. Third, we note that the window t_w itself acts as a filter. This is the case because frequencies $f\geq t_w^{-1}$ are not resolved by the range of time scales included within the window. In effect, simply increasing the window from $t_w=t'$ to $t'+\Delta t$ serves to filter the data in the frequency range $1/t'$ to $1/(t'+\Delta t)$. This effect is clearly evidenced in the correlation integral plots given below.

We refer to Grassberger and Procaccia for the definition of order-q fractal dimension (see Eqs. (3.3) and (3.4) in Grassberger and Procaccia [16]). Approximations of correlation integrals using discrete data are calculated using the formula

$$C_q(r)=\left[(1/N)\sum_{j=1}^{N}(n_j(r))^{q-1}\right]^{1/q-1} , \tag{3.5}$$

where $C_q(r)$ is the correlation integral for the embedded data, r is the observing length scale in E^n, q is a nonnegative real variable, N is the number of points in the embedding space, and $n_j(r)$ is the fraction of embedded points surrounding point $p(j)$ within the observing radius r. If the correlation integral has exponential structure

$$C_q(r)\propto r^{D_q} \tag{3.6}$$

over some range of length scales r, then D_q is the order-q fractal dimension of the attractor. The fractal dimension corresponding to $q=2$ is referred to in the literature as the correlation dimension [6,16]. The correlation integrals presented in this paper are for $q=2$.

B. Filtering affects on correlation integrals

We look at a sample of correlation integrals calculated for reconstructed attractors using measured time-series data and compare those results to ones obtained after moving the filter-cutoff point. In particular, we use the power spectrums of those time series to guide our choices for window length. In the last part of this section we show the length scale range for analyzing fractal structure can be estimated by examining the singular values of the trajectory matrix.

We begin by noting the contrast between the spectral density curves for the measured fluidized-bed data (Fig. 2) and those for the Franceschini- and Lorenz-model data [Figs. 3(a) and 3(d)]. Specifically, we point to the background in Fig. 2. Recall that the cutoff frequency for the fluidized-bed measurements is 40 Hz. The rolloff at 40 Hz due to the filter is clearly visible in Fig. 2. It is also clear in Fig. 2 that the frequency content of the background is not well separated from that of the two experimental conditions for frequencies higher than approximately 25 Hz. Using that separation as a guideline, we set

$$t_n^{-1}=25 \text{ Hz} \tag{3.7}$$

for the two sets of fluidized-bed data. Following Broomhead and King, for the Lorenz and Franceschini data sets, respectively, we tentatively set $t_n^{-1}=20$ and 150 Hz, which in each case is about where the power spectrum reaches the noise floor.

We test the values for t_n selected above by looking at correlation integrals for a series of reconstructed attractors. Figures 5(a) and 6(a) show correlation integral analyses for the two fluidized-bed measured time series over a range of window lengths t_w. Similarly, Figs. 7(a) and 8(a) display correlation integrals for the Lorenz and Franceschini data. Table I shows singular values for one case from each of the four figures 5(a), 6(a), 7(a), and 8(a). The embedding dimension for each of those cases is $n=10$. The first of the two fluidized-bed cases ($v=2.4$ m/s) is labeled FB_1 and the second ($v=5.7$ m/s) FB_2, while the Lorenz and Franceschini cases are labeled L and F, respectively.

We observe that for both fluidized-bed experimental conditions the correlation integrals for the reconstructed attractors converge approximately where $t_w \approx t_n$. For both the Lorenz- and Franceschini-model cases, the correlation integrals appear to converge at approximately the frequency where the spectral density curve begins to change slope before merging with the noise floor. For the Lorenz case, that transition point is approximately $t_w^{-1} \approx 10$ Hz, while for the Franceschini case it appears to be $t_w^{-1} \approx 110$ Hz. We note that those frequencies each mark the point where there is approximately an order of magnitude difference in power relative to the noise floor.

Next, we look at the effect on the analysis of shifting the filter-cutoff point. We start with the Lorenz case. Recall that Fig. 4(c) displays spectral density curves corresponding to the Lorenz data successively filtered using cutoff values $f=166$, 6, 3, and 1.5 Hz. Figure 7(b) shows the result of analyzing correlation integrals for attractors reconstructed using the parameter values $(k,n)=(5,10)$, which corresponds to $t_w^{-1}=7.4$, for the first three cutoff

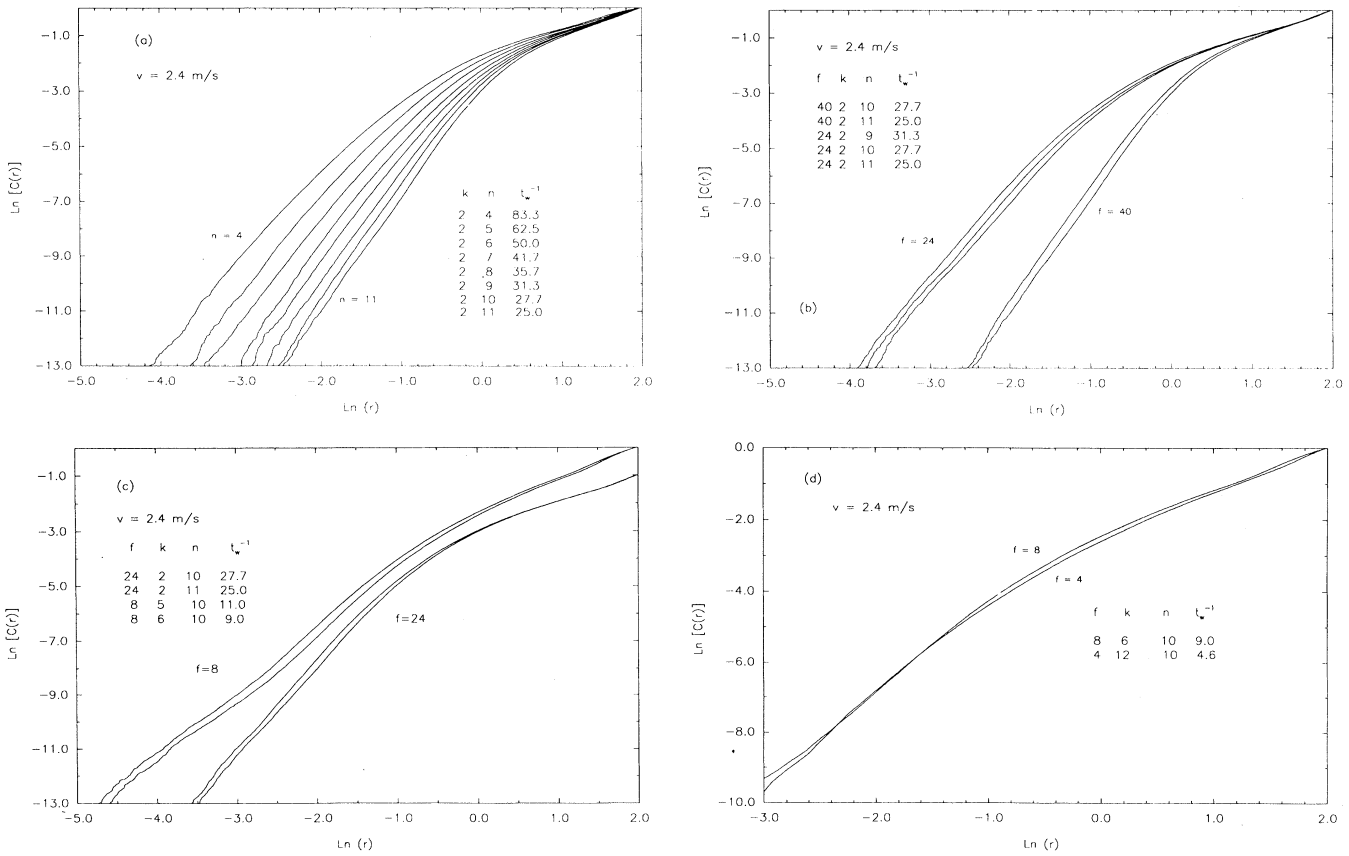

FIG. 5. Fluidized-bed correlation integrals ($v=2.4$ m/s): (a) $f=40$ Hz; (b) $f=40$ and 24 Hz; (c) $f=24$ and 8 Hz; (d) $f=8$, and 4 Hz.

TABLE I. Singular values ($n=10$) for four cases. Note: $0.aaaa[n]=0.aaaa\times 10^{n}$.

Index \ $k=$	FB_1 2	FB_2 2	L 4	F 1
1	0.2642[2]	0.2459[1]	0.5911[3]	0.2232[3]
2	0.9892[0]	0.5060[0]	0.2927[2]	0.4433[1]
3	0.9396[−1]	0.7174[−1]	0.1048[1]	0.7899[−1]
4	0.1432[−1]	0.1185[−1]	0.2849[−1]	0.2517[−2]
5	0.1834[−2]	0.1566[−2]	0.7670[−3]	0.4572[−4]
6	0.1726[−3]	0.1368[−3]	0.1796[−4]	0.2394[−5]
7	0.8294[−5]	0.7133[−5]	0.4570[−6]	0.5857[−6]
8	0.3177[−6]	0.2631[−6]	0.7514[−7]	0.4879[−6]
9	0.8431[−8]	0.6568[−8]	0.6673[−7]	0.4835[−7]
10	0.2461[−9]	0.1881[−9]	0.6596[−7]	0.4631[−7]

values $f=166$, 6, and 3. The results are virtually identical. Now consider the analysis of the Lorenz measured data filtered using the cutoff point $f=1.5$ Hz. Figure 7(c) displays correlation integrals for reconstructed attractors corresponding to the fixed embedding dimension $n=10$ and the range of time lags $k=5$, 10, and 15, which determines the range of window frequencies $t_w^{-1}=7.4$, 3.7, and 2.5. If the correlation integral from Fig. 7(c) corresponding to the window frequency $t_w^{-1}=2.5$ Hz were added to Fig. 7(b), it would be indistinguishable from the plots in that figure over the range $-2.0\leq \ln r\leq 2.0$. In Fig. 7(b), the slope of the correlation integral over the range $-4.0\leq \ln r\leq -2.0$ is approximately $s=2.05$, which is the correlation dimension normally reported in the literature [6]. There is a second range of fractal structure corresponding approximately to $-2.0\leq \ln r \leq 1.0$, where the correlation dimension is approximately $s=1.8$. We note from Fig. 7(c) that the fractal structure for the second range of length scales is retained in the data filtered using the cutoff frequency $f=1.5$, but that

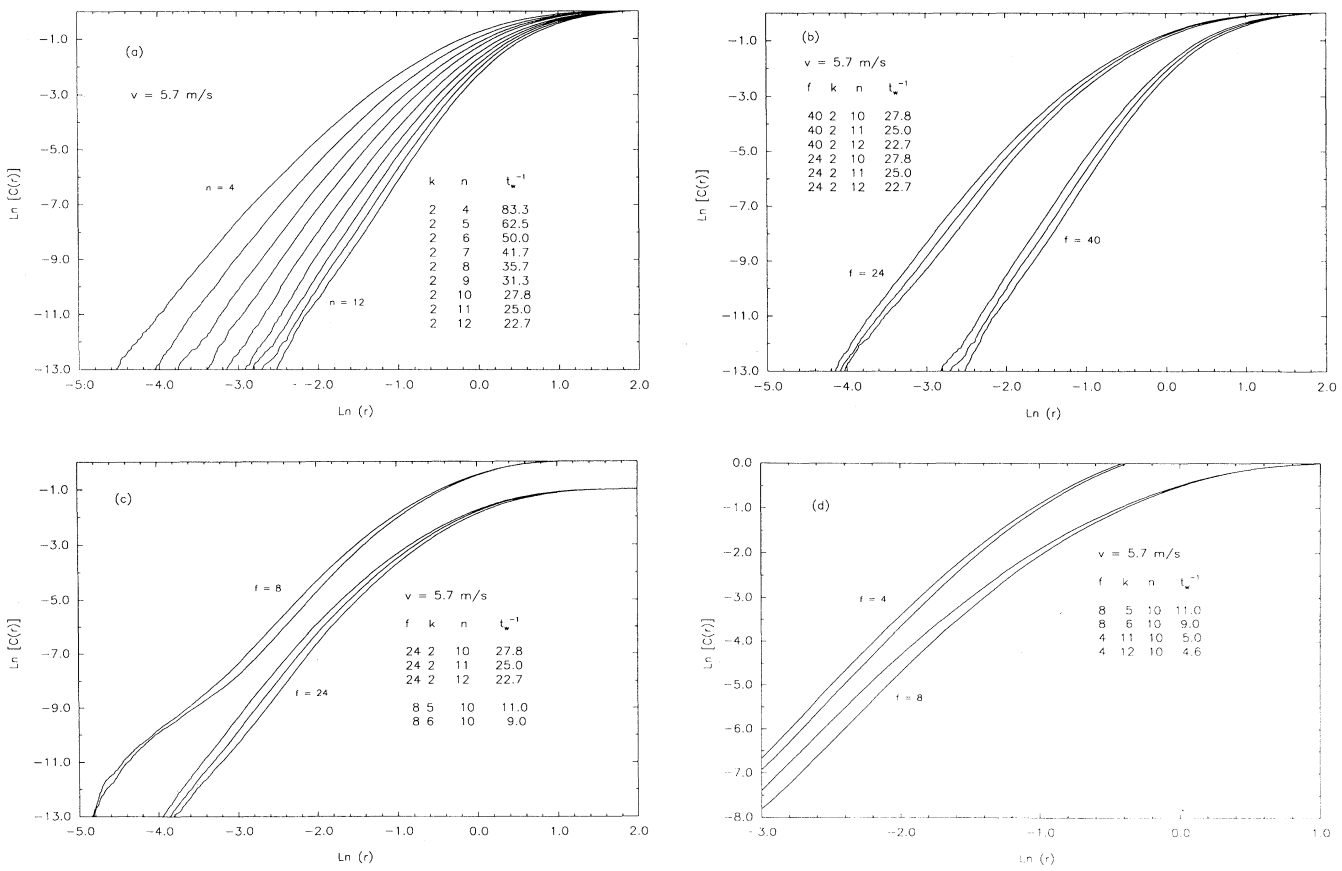

FIG. 6. Fluidized-bed correlation integrals ($v=5.7$ m/s): (a) $f=40$ Hz; (b) $f=40$, and 24 Hz; (c) $f=24$ and 8 Hz; (d) $f=8$ and 4 Hz.

TABLE II. Fluidized-bed singular values ($v=2.4$ m/s, $n=10$) for one case from each of four filter settings. Note. $0.aaaa[n]=0.aaaa\times 10^{n}$.

Index \ $f=$ / $k=$	40 / 2	24 / 2	8 / 6	4 / 12
1	0.2642[2]	0.2574[2]	0.1676[2]	0.6255[1]
2	0.9892[0]	0.7346[0]	0.2487[1]	0.3397[1]
3	0.9396[−1]	0.3295[−1]	0.5408[−1]	0.7173[−1]
4	0.1432[−1]	0.2763[−2]	0.6103[−2]	0.8313[−2]
5	0.1834[−2]	0.2127[−3]	0.5422[−3]	0.6728[−3]
6	0.1726[−3]	0.1795[−4]	0.6906[−4]	0.9857[−4]
7	0.8294[−5]	0.8072[−6]	0.8763[−5]	0.1584[−4]
8	0.3177[−6]	0.2748[−7]	0.1611[−5]	0.2919[−5]
9	0.8431[−8]	0.1103[−8]	0.3426[−6]	0.5558[−6]
10	0.2461[−9]	0.5535[−7]	0.1115[−7]	0.1515[−6]

the fractal structure in the smaller length scale range appears to be lost.

Figure 4(c) illustrates the spectral density curves for the Franceschini-model data using the filter-cutoff values $f=250$, 50, and 30, and Fig. 8(b) displays correlation integrals over the length scale range $-2.0\le \ln r\le 2.0$ for three attractors constructed using those filtered data sets. In each of those cases we use the parameter values $(k,n)=(4,10)$. For those parameter values $t_w^{-1}=27.7$. Without showing the plot, we make note that the correlation integral for the measured Franceschini data, where $f=500$, using those same parameter values for lag time and embedding dimension is indistinguishable from the result using the data filtered at $f=250$. The slope of the correlation curve corresponding to $n=10$ in Fig. 8(a) is approximately $s=1.18$, whereas the three curves in Fig. 8(b) each have the approximate slope $s=1.05$. Using the same filtered data sets, we set $(k,n)=(3,10)$, which determines $t_w^{-1}=37.0$, and again calculate the correlation integrals. The results are displayed in Fig. 8(c). A second region of fractal structure, now for the length scale range $-4.0\le \ln r\le -2.0$, is evidenced in Fig. 8(c).

We now consider the filtered fluidized-bed data. First, we look at the case $v=2.4$ m/s. Table II contains singular values for one case corresponding to each of the four filter settings, $f=40$, 24, 8, and 4. Figure 5(b) illustrates correlation integrals for three reconstructed attractors using data filtered at $f=24$ superimposed with two correlation integrals for $f=40$. The two correlation integrals for $f=40$ are also presented in Fig. 5(a). We note from Fig. 5(b) that for the approximate range $-2.5\le \ln r\le -1.5$ both sets of correlation integrals are linear and that the slope of the more highly filtered family is less than that for the other. Further, we note there appears to be a second region of linearity, which is more visible for the $f=24$ family, over the length scale range $0.0\le \ln r\le 2.0$. Figure 5(c) displays plots of correlation integrals for reconstructed attractors corresponding to the filter-cutoff points $f=24$ and 8. The two case for $f=24$ are also plotted in Fig. 5(b), but in Fig. 5(c) they are translated one unit along the ordinate so that the two families of curves can be clearly distinguished. Note again there appear to be two regions of linearity. In the neighborhood of $\ln r=-2.0$, the slope of the $f=8$ family is approximate to, but less than, the slope of the $f=24$ family. In Fig. 5(c) the linearity over the range $0.0\le \ln r\le 2.0$ is much more well defined for the more highly filtered family. Finally, Fig. 5(d) shows plots of correlation integrals for attractors constructed using the filter-cutoff points $f=8$ and 4. The scales for Fig. 5(d) are chosen so to magnify the features of the correlation integrals over $-3.0\le \ln r\le 2.0$. We note that both fami-

TABLE III. Fluidized-bed singular values ($v=5.7$ m/s, $n=10$) for one case from each of four filter-cutoff values. Note: $0.aaaa[n]=0.aaaa\times 10^{n}$.

Index \ $f=$ / $k=$	40 / 2	24 / 2	8 / 6	4 / 12
1	0.2459[1]	0.2089[1]	0.7088[0]	0.2040[0]
2	0.5060[0]	0.2978[0]	0.2265[0]	0.1299[0]
3	0.7174[−1]	0.2278[−1]	0.2523[−1]	0.1299[−1]
4	0.1185[−1]	0.2035[−2]	0.3451[−2]	0.2616[−2]
5	0.1566[−2]	0.1855[−3]	0.3528[−3]	0.3351[−3]
6	0.1368[−3]	0.1416[−4]	0.4780[−4]	0.6307[−4]
7	0.7133[−5]	0.6860[−6]	0.7422[−5]	0.1083[−4]
8	0.2631[−6]	0.2195[−7]	0.1362[−5]	0.1957[−5]
9	0.6568[−8]	0.4661[−9]	0.2832[−6]	0.3945[−6]
10	0.1881[−9]	0.7436[−9]	0.5872[−7]	0.1071[−6]

lies appear to display the same structure in that range of length scales.

Now we consider the fluidized-bed case $v=5.7$ m/s. Table III contains singular values for one case from each of the four time series obtained using the filter-cutoff values $f=40$, 24, 8, and 4. Figure 6(b) displays three correlation integrals from each of the two families of reconstructed attractors corresponding to $f=40$ and 24, where the correlation integrals for $f=40$ are also displayed in Fig. 6(a). The linearity of the two families of correlation integrals is clearly evidenced by the plots in Fig. 6(b) and, further, we note that the slopes of those families are more nearly equal than for the corresponding pair in Fig. 5. Again, the slope of the family constructed using the more highly filtered time series is less than that for the other family. Figure 6(c) corresponds to Fig. 5(c). The correlation integrals displayed in those figures derive from the time series obtained using the filter settings $f=24$ and 8 and, as in Fig. 5(c), the integrals for the $f=24$ family are translated one unit along the ordinate

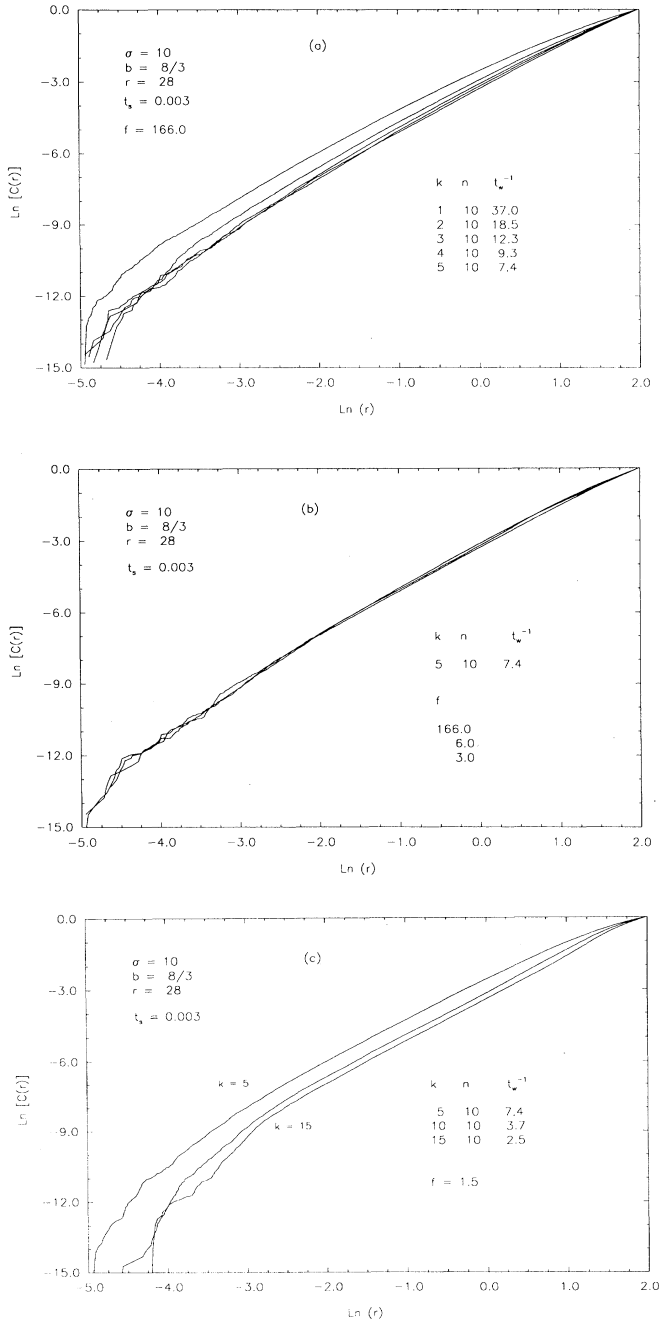

FIG. 7. Lorenz model correlation integrals: (a) $f=166$ Hz; (b) $f=166$, 6, and 3 Hz, $t_w^{-1}=7.4$; (c) $f=1.5$ Hz.

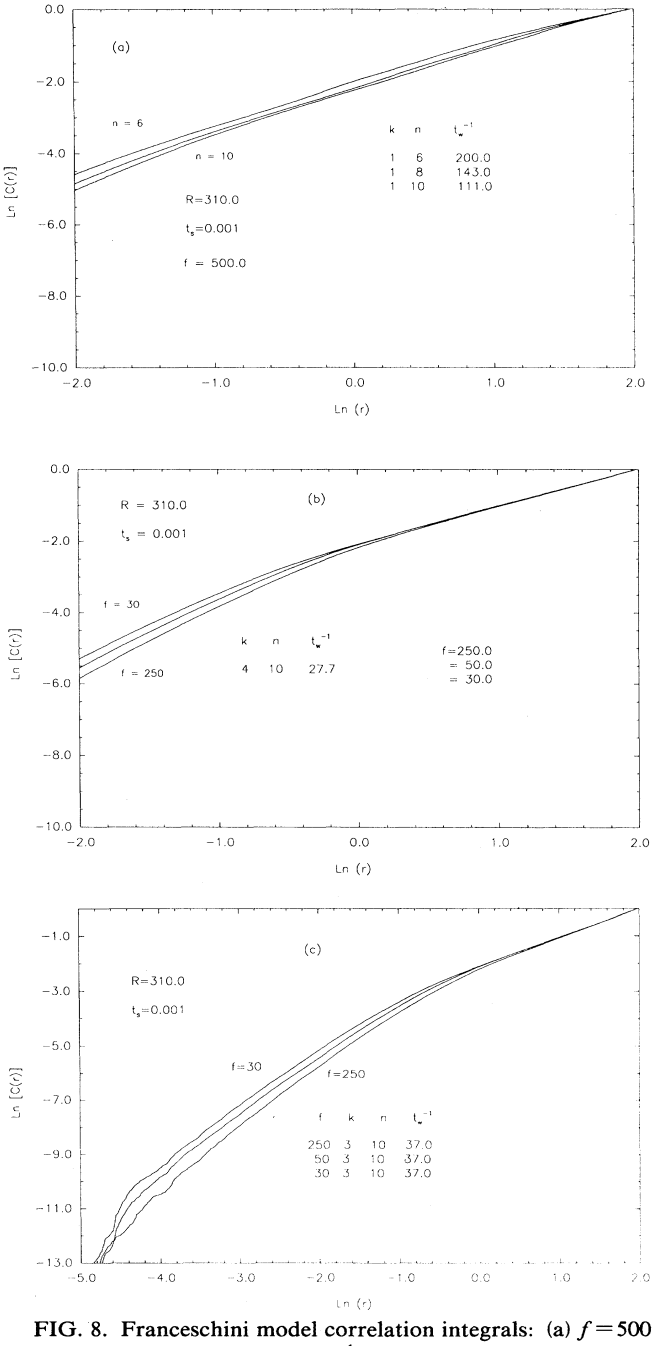

FIG. 8. Franceschini model correlation integrals: (a) $f=500$ Hz; (b) $f=250$, 50, and 30 Hz, $t_w^{-1}=27.7$; (c) $f=250$, 50, and 30 and Hz, $t_w^{-1}=37.0$.

TABLE IV. Fluidized-bed correlation dimensions.

	D_2	
f	$v=2.4$ (m/s)	$v=5.7$ m/s
40	4.06	3.78
24	3.38	3.74
8	2.79	3.06
4	2.75	3.77

for the purpose of clarity. The $f=8$ family appears to have linear structure for length scales in a neighborhood of $\ln r=-2.5$ and the slope for the family approximates the slope for the $f=24$ family. Again we make a comparison with the corresponding pair of families of correlation integrals for the case $v=2.4$ m/s, Fig. 5(c), and note that for the higher-velocity case the slopes of the two families are more nearly equal than for the lower-velocity case. Figure 6(d) shows correlation integrals calculated using time series obtained by filtering the measured data with the filter settings $f=8$ and 4. Figure 6(d) corresponds to Fig. 5(d). Even for filter-cutoff value $f=4$, the correlation integrals continue to display a linear structure in a neighborhood of $\ln r=-2.5$. However, there is a marked difference in that structure for the two experimental conditions over the higher length scale range. The $v=5.7$ m/s case does not display fractal structure for the larger length scales, whereas the $v=2.4$ m/s case does.

Table IV is a summary of correlation dimensions estimated from the correlation integrals for the fluidized-bed data presented in Figs. 5 and 6. For the case $v=2.4$ m/s, note the correlation dimension D_2 appears to decrease with decreasing f over the range of filter-cutoff values used in this study. Except for the filter-cutoff value $f=8$ Hz, the correlation dimension is invariant with f for the case $v=5.7$ m/s. We point out for future reference that this relationship between f and D_2 for the case $v=2.4$ m/s is not consistent with the results of Baddii *et al.* [7] and Mitschhe, Moller, and Lange [8]. We will elaborate on this point in Sec. IV.

C. Effects of filtering on the observable dynamics

We want to analyze the effect of filtering and window length on the attractor reconstruction process. The correlation integral is used as a quantitative observable of that process. We analyze the dependence of the correlation integral on the filter-cutoff value f and the window t_w by, first, looking at the effect of those parameters on the singular values of the correlation matrix Eq. (3.4) and, second, relating changes in those singular values to changes in a correlation integral. Figures 9(a)–9(f) are singular value analyses for the two fluidized-bed cases, and Figs. 9(g) and 9(h) are singular value studies for the Lorenz and Franceschini cases. In the transformed coordinates based on the singular value analysis of the correlation matrix Eq. (3.4), the length scale of the reconstructed attractor in a given coordinate direction is $r=\sigma^{1/2}$, where σ is the corresponding singular value. Figure 10 is a graph showing how length scales r relate to singular values σ.

First, consider the fluidized-bed data. Referring to Figs. 9(a) and 9(b), with the filter frequency fixed at $f=40$ and the window defined so that $t_w^{-1}\approx 40$, the singular values for the two experimental conditions are virtually identical; in fact, if the two plots were overlayed, they would be indistinguishable. Figures 9(a) and 9(b) also illustrate that, with the filter frequency fixed at $f=40$, moving the window frequency from $t_w^{-1}\approx 40$ to $t_w^{-1}\approx 25$ causes the singular values to be amplified. The two cases $f=40$ and $t_w^{-1}\approx 25$ from Figs. 9(a) and 9(b) are plotted together in Fig. 9(c). Those singular value plots appear to asymptotically converge and are virtually identical for singular value indices ≥ 4. Using Fig. 10, the first six singular values correspond approximately to the length scale range $-5.0\leq \ln r\leq 2$. We note that is the length scale range used for all the frames in Figs. 5 and 6 except those showing results for the filter cutoff $f=4$. Referring to Figs. 5(a) and 6(a), note that the correlation integrals appear linear only for length scales $\ln r>-2.5$, which corresponds in both cases to singular value indicies ≤ 4.

Next, consider the effect of moving the filter cutoff from $f=40$ to 24 while leaving the window frequency value fixed at $t_w^{-1}\approx 25$. Figures 9(a) and 9(b) show that, for both experimental conditions, the singular values are reduced in magnitude, but for each case the ratio of corresponding singular values, viewed as a function of singular value index, varies from 1 to an approximately constant value for indicies ≥ 3. The two singular value plots from Figs. 9(a) and 9(b) for the conditions $f=24$ and $t_w^{-1}\approx 25$ are also displayed in Fig. 9(c). They appear to asymptotically converge at the index value 5. The correlation integrals corresponding to the cases $f=40$ and 24 and $t_w^{-1}\approx 25$ are included in Figs. 5(b) and 6(b). We note that for both examples the correlation integral for $f=24$ is approximately equal to a translation of the correlation integral for $f=40$ and, further, that the stretching, or distortion, for the range of length scales corresponding to singular values 1–3 is less for the $v=5.7$ m/s case than for the $v=2.4$ m/s case. The translation in each case corresponds to the constant ratio value of corresponding singular values. We note from Figs. 9(a) and 9(b) that the variation in ratios of singular values for $f=40$ and 24 over indices 1–3 is smoother for the case $v=5.7$ m/s than for the case $v=2.4$ m/s.

Figures 9(d) and 9(e) illustrate singular values for one reconstructed attractor corresponding to each of the filter-cutoff values $f=40$, 24, 8, and 4 for each of the two experimental conditions. Further, each of the analysis given in those figures correspond to one of the correlation integrals in Figs. 5 and 6. Recall that in Figs. 5(c) and 7(c) the $f=24$ family is translated along the ordinate for clarity. Note that in Figs. 5 and 6 for each of the cases $f<40$, the window frequency $t_w^{-1}\approx f$.

First, consider the case $v=2.4$ m/s. Referring to Fig. 9(d), the ratio of singular values 3 and 4 for the pair $f=8$ and 24 appears to be approximately a constant times the ratio of the same singular values for $f=40$ and 24. The length scale range for singular values 3 and 4 is approxi-

mately $-2.5 \leq \ln r \leq -1$. From Fig. 5(c), we note the similarity in correlation integrals over those length scales for the families $f=24$ and 8 and note, also, that information on fractal structure for length scales corresponding to the fifth singular value is lost in the $f=8$ family. In contrast, Fig. 9(d) shows there is a significant difference in the ratios of singular values 1–3 for the pairs $f=40$ and 24 and $f=8$ and 24. As a result of moving the filter value from $f=24$ to 8, the second singular value is amplified and the ratio of the second to first singular value is significantly magnified. As noted earlier, the linear structure for length scales $\ln r > 0$, which corresponds to singular values 1 and 2, is more clearly observable for the $f=8$ family than for the $f=24$ family. In

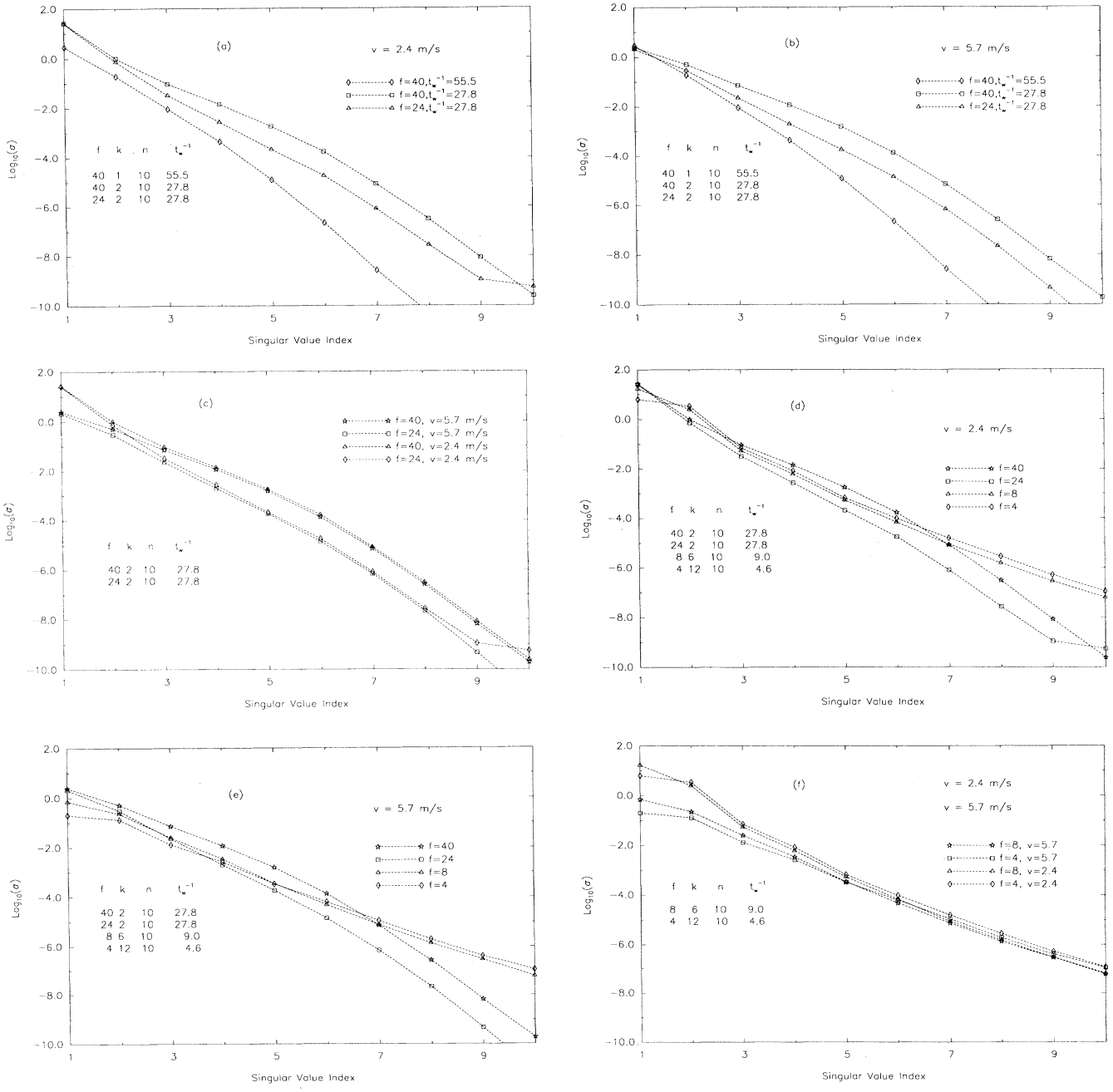

FIG. 9. Singular values: (a) fluidized-bed data, $v=2.4$ m/s, $f=40$ and 24; (b) fluidized-bed data, $v=5.7$ m/s, $f=40$ and 24; (c) fluidized-bed data, $v=2.4$ and 5.7 m/s, $f=40$ and 24; (d) fluidized-bed data, $v=2.4$ m/s, $f=40$, 24, 8, and 4; (e) fluidized-bed data, $v=5.7$ m/s, $f=40$, 24, 8 and 4; (f) fluidized-bed data, $v=2.4$ and 5.7 m/s, $f=8$ and 4; (g) Lorenz data, $f=166$, 6, 3, and 1.5; (h) Franceschini data, $f=500$, 250, 50 and 30.

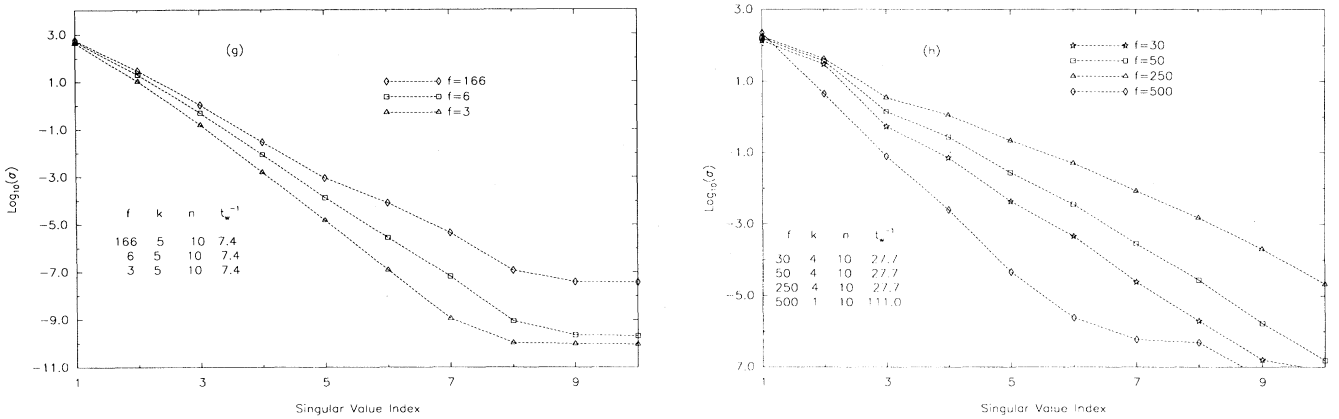

FIG. 9. (*Continued*).

going from the filter value $f=8$ to $f=4$, the second singular value is magnified relative to the first, but the correlation integrals, Fig. 5(d), are affected very little for length scales $\ln r \geq -2.5$.

Now consider the case $\nu=5.7$ m/s. From Fig. 9(e), except that the second singular value is magnified relative to the first in going from $f=24$ to $f=8$, singular values 1–5 are very similar. We note from Figs. 6(b) and 6(c) that the correlation integrals for the families $f=40$, 24, and 8 are translations of one another over the length scale range $-3.5 \leq \ln r$. We also note that the fifth singular value corresponds to $\ln r \approx -3.5$. Again referring to Fig. 9(e), note that singular values 1–4 for $f=8$ and $f=4$ vary very similarly, although the fourth is magnified relative to the third in making the change. The fourth singular value for those filter-cutoff values corresponds to the length scale $\ln r \approx -3$. Referring to Fig. 6(d), recall that the $f=4$ family is translated $\frac{1}{2}$ unit along the ordinate, again for clarity. The two families of correlation integrals in that figure are very similar, but the slope of the $f=4$ family is greater than that for the $f=8$ family for the range of length scales corresponding to the third and fourth singular values.

Figure 9(f) shows together the singular value plots from Figs. 9(b) and 9(c) for the filter values $f=8$ and 4.

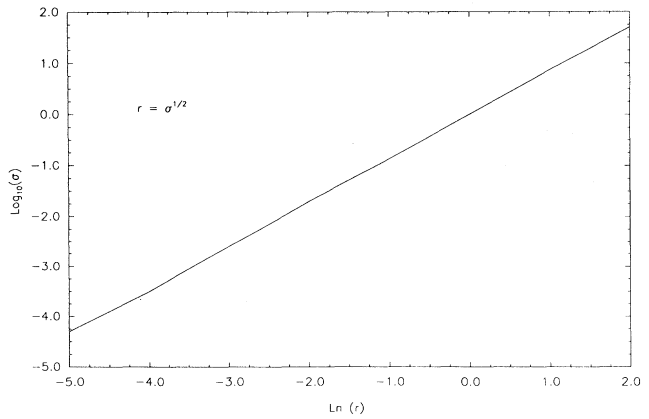

FIG. 10. Relationship between singular values and length scales.

The pairs corresponding to the two experimental conditions are clearly distinguishable in that figure for indices 1–5, but it is also evident in that figure that the plots do not differ significantly for indices ≥ 5. Recall Fig. 9(c). Figure 9(c) illustrates that the two pairs of plots from Figs. 9(a) and 9(b) corresponding to the conditions $f=40$ and $t_w^{-1} \approx 25$, and $f=24$ and $t_w^{-1} \approx 25$, respectively, have the property that the singular values in each pair converge asymptotically and are indistinguishable for indices ≥ 4. We also recall that the two singular value plots from Figs. 9(a) and 9(b) corresponding to $f=40$ and $t_w^{-1} \approx 40$ are virtually identical. An explanation for these observations is that the singular values with indices ≥ 5 are dominated by background processes.

Figure 9(g) shows singular values for the Lorenz case and Fig. 7 shows correlation integrals for the Lorenz data. Note from Fig. 7(b) that the fractal structure of the Lorenz data corresponds to length scales $\ln r \geq -4$ and from Figs. 9(e) and 10 that those length scales correspond approximately to the first five–six singular values. The ratio of singular values 1–6 corresponding to one pair of filter values differs from that of any other pair by approximately a scale factor. As noted earlier, there is virtually no change in the correlation integrals.

Figure 9(h) shows singular values for the Franceschini case, and Fig. 8 shows correlation integrals for the Franceschini data. Recall that in Fig. 8(b) the filtered data sets are analyzed using the window frequency $t_w^{-1}=27.7$, while in Fig. 8(c) the same data sets are analyzed using $t_w^{-1}=37.0$. In Fig. 9(h) we use the same lag time and embedding dimension for the filtered data sets as used in Fig. 8(b). Without showing the plots, we note that the singular value structure for the filtered data sets using the lag time and embedding dimension used in Fig. 8(c) is the same as that in Fig. 9(h). With the window frequency $t_w^{-1} \approx 30.0$, Figs. 8(b) and 8(c) illustrate that the correlation integral is insensitive to variations in the filter-cutoff point over the range $30 \leq f \leq 500$.

To conclude this section, we briefly consider one additional aspect of the reconstruction process as relates to principal component analysis and filtering. Singular value analysis of the trajectory matrix Eq. (3.4) provides a global means for projecting the reconstructed attractor in E^n onto a least-squares approximation of that attractor

contained in a linear subspace of E^n. To be specific, after making the transformation to the basis of E^n defined by the eigenvectors of the correlation matrix Eq. (3.4), we project the attractor into the linear subspace spanned by the eigenvectors corresponding to eigenvalues greater than the noise floor value. Referring to a remark made earlier in this section, qualitatively this has the effect of smoothing the "skin thickness" of the attractor in the coordinate directions associated with the noisy eigenvalues. This projection does not effect the fractal structure of the attractor, since it only acts on length scales associated with noise in the process. For example, consider Fig. 5(b). That figure shows several correlation integrals for attractors constructed using the fluidized-bed data $v=2.4$ m/s. One of those correlation integrals is for the case $f=24$ and the reconstructed attractor obtained using the parameter values $(k,n)=(2,10)$. If we were to add to Fig. 5(b) the correlation integral calculated using the approximate attractor obtained by projecting that attractor into the six-dimensional linear subspace of E^{10} corresponding to the first six principal components (see Table I), the two integrals would be virtually indistinguishable.

IV. SUMMARY AND CONCLUSIONS

The primary objective of the work presented in this paper is to investigate the Broomhead and King approach for implementing Takens's method of delays using experimental data obtained under realistic measurement conditions. Under such conditions, it can be expected that the background environment where the experiment, or engineering process, is conducted will contribute to the frequency content of the measured observable.

Filtering is an important aspect of all forms of data measurement. In particular, low-pass filters are incorporated in time-series measurement devices to mitigate Nyquist folding. We investigate the relationship between the low-pass filter-cutoff point f, the Broomhead and King window frequency t_w^{-1}, and the background process. Further, we study the effect on attractor reconstruction of varying the filter-cutoff frequency over a wide range of values. One reason for doing this is to investigate whether the filter, by means of moving the filter-cutoff frequency, can be used as a diagnostic tool for studying the structure of the attractor.

The experimental data used in this paper are time-series pressure measurements from a laboratory fluidized bed. We use data corresponding to two very distinct experimental conditions. Also, we have data for the null experimental condition, that is, the case where the fluidized bed is not in operation. That data serve to represent the background. We also use data obtained from two model systems of ordinary differential equations, the Lorenz and Franceschini models. The primary motivation for including model data in our study is to see whether there are significant differences between analyzing experimental and model data.

The fluidized-bed data are measured using a low-pass filter-cutoff value $f=40$ Hz. From the spectral density curves for the experimental data, Fig. 2, it is clear that the background is not distinguishable from the fluidized-bed process for frequencies greater than $t_n^{-1}\approx 25$ Hz. It appears from the correlation integral studies [Figs. 5(a) and 6(a)] that a necessary condition for convergence is that the Broomhead and King window frequency $t_w^{-1}\approx t_n^{-1}$. As illustrated in Fig. 9(c), moving the filter cutoff from 40 to 24 Hz has a very similar effect on the singular values for both cases. For both cases, the singular values of order three and higher are decreased significantly. However, as shown in Table IV and illustrated in Figs. 5(b) and 6(b), the result of moving the filter frequency on the estimated correlation dimension is different for the two cases. For the case $v=5.7$m/s, there is a shift in the length scale range of fractal structure, which corresponds to the decrease in the singular values, but the fractal structure is unchanged. For the case $v=2.4$ m/s, there is the same shift in the range of fractal structure, but the dimension changes from $D_2\approx 4.06$ to $D_2\approx 3.38$. Referring again to Fig. 9(c), looking at the ratio of higher-order singular values to the first singular value and considering the change with the filter-cutoff point, for the case $v=2.4$ m/s the relative decrease in singular values 3 and 4 is significantly greater than for the case $v=5.7$ m/s. Turning to the model data, in both cases we find the correlation integrals converge at approximately the window frequency where there is an order of magnitude difference in the power of the process and the power of the noise floor (see Figs. 3, 7, and 8).

We study the effect on the attractor-reconstruction process of varying the filter-cutoff point from 24 to 4 Hz by first looking at the effect of moving the filter value on correlation integrals and then relating that effect to observed changes in the singular values of the correlation matrix Eq. (3.1). In those studies the window frequency is moved so that the condition $t_w^{-1}\approx f$ is maintained. From Fig. 2, we note the spectral density for the fluidized bed case $v=5.7$ m/s is significantly more broadband than that for the case $v=2.4$ m/s. Table IV summarizes correlation dimension values as parametrized by the filter-cutoff frequency for the two fluidized-bed cases. Those results also serve to distinguish the two fluidized-bed regimes. With reference to Figs. 5 and 6, for both cases high frequencies contribute to small length scale structure in the correlation integrals, so that as the cutoff frequency is lowered the minimum resolved length scale increases. Consider the case $v=5.7$ m/s. It appears that frequencies lower than the cutoff frequency contribute information about fractal structure to each of the singular coordinate directions and that, while the minimum length scale of resolution increases, the information contribution to each degree of freedom is invariant with the cutoff frequency. Consider, however, the case $v=2.4$ m/s. The results for this case imply that, as the cutoff frequency is decreased, information about fractal structure is increasingly removed from the significant lowest-order degrees of freedom. The singular value analyses, again parametrized by the cutoff frequency, serve to further discriminate between the two cases. For instance, a comparison of Figs. 9(d) and 9(e) illustrates that there is a difference between the two cases insofar as how the significant singular values, those with indices 1–5, vary

with the cutoff frequency. For the case $v=5.7$ m/s, as the cutoff frequency varies from 24 to 4 Hz, there is very little variation in the singular values corresponding to the length scale range of fractal structure. On the other hand, for the case $v=2.4$ m/s, there is a significant increase in the second singular value as the cutoff frequency is moved from 24 to 8 Hz and, from Table IV, the estimated dimension changes from $D_2=3.38$ to $D_2=2.79$.

We summarize the model studies. Concerning the Lorenz data, moving the filter-cutoff value has little effect on the structure of the singular value spectrum, Fig. 9(g), and, in turn, little effect on the correlation integrals, Fig. 7. Referring to Fig. 8 for correlation integrals and Fig. 9(h) for singular value analyses, the Franceschini-data analyses are also insensitive to wide variations in the filter-cutoff value.

We want to relate the window frequency condition $t_w^{-1}\approx f$ to the discussion of filters by Broomhead, Huke, and Muldoon [9]. For frequencies higher than the cutoff frequency f, a filter produces noise. Therefore, if $t_w^{-1}>f$, the window used for the reconstruction process includes information produced by the filter, and hence we would expect the resulting dimension to be greater than that for the process represented only by frequencies less than the filter-cutoff frequency f. This is consistent with the fluidized-bed analyses presented in this paper in that we did not see convergence in the correlation integral while $t_w^{-1}>f$. In effect, Broomhead, Huke, and Muldoon [9] are also imposing the condition $t_w^{-1}\approx f$ in their argument regarding the approximation of a recursive filter by a nonrecursive one. Recall the expression (2.5),

$$y_{i+1}=a^n y_{i-n}+\sum_{j=0}^{n-1} a^j b x_{i-j} ,$$

where

$$a=\exp(-2\pi f t_s) .$$

The condition $a^n\approx 0$, where n is the order of the nonrecursive filter that is equivalent to the recursive filter, is essentially equivalent to the window frequency condition $t_w=(n-1)t_s\approx f^{-1}$, where now n is the embedding dimension. Broomhead, Huke, and Muldoon [9] are imposing the condition on the reconstruction process that the attractors constructed using the filtered data y and the unfiltered data x are equivalent provided $t_w^{-1}\approx f$. In turn, they argue that if the order of the nonrecursive filter n, which is also the required embedding dimension, is large, then a large amount of data is needed to resolve the reconstructed attractor and, hence, to analyze the dimension.

Takens's reconstruction theorem together with the results of Broomhead, Huke, and Muldoon [9] implies that data corresponding to frequencies less than the filter-cutoff frequency can, in principle, provide all the information needed for the reconstruction process. The questions that remain are, first, how much data is needed and, second, what is the accuracy requirement for that data? Broomhead, Huke, and Muldoon [9] point to limited amounts of data as a cause for inaccurate estimates of dimension, particularly in reference to large values of the embedding dimension. The fluidized-bed studies presented in this paper are all based on one data set size, namely, 2×10^4 points, and a fixed data-measurement accuracy criterion. Given those conditions, the effect of moving the filter-cutoff point on the analysis of the two very distinct fluidized-bed regimes is significant.

[1] F. Takens, in *Proceedings of the Warwick Symposium, 1981,* edited by D. A. Rand and L. S. Young (Springer, New York, 1981).

[2] C. S. Daw, W. F. Lawkins, D. J. Downing, and N. E. Clapp, Jr., Phys. Rev. A **41**, 1179 (1990).

[3] E. N. Lorenz, J. Atmos. Sci. **20**, 130 (1963).

[4] V. Franceschini, Physica **6D**, 285 (1983).

[5] D. S. Broomhead and G. P. King, Physica **20D**, 271 (1986).

[6] P. Grassberger and I. Procaccia, Physica **9D**, 189 (1983).

[7] R. Badii, G. Broggi, B. Derighetti, M. Ravani, S. Ciliberto, A. Politi, and M. A. Rubio, Phys. Rev. Lett. **60**, 979 (1988).

[8] F. Mitschke, M. Moller, and W. Lange, Phys. Rev. A **37**, 4518 (1988).

[9] D. S. Broomhead, J. P. Huke, and M. R. Muldoon, J. R. Stat. Soc. B **54**, 373 (1992).

[10] A. M. Fraser and H. L. Swinney, Phys. Rev. A **33**, 1134 (1986).

[11] A. M. Fraser, Physica **34D**, 391 (1989).

[12] J. S. Bendat and A. G. Piersol, *Random Data: Analysis and Measurement Procedures* (Wiley, New York, 1971).

[13] B. L. Buzbee, in *Sources and Development of Mathematical Software,* edited by W. R. Cowell (Prentice-Hall, Englewood Cliffs, NJ, 1984).

[14] L. F. Shampine and M. K. Gordan, *Computer Solution of Ordinary Differential Equations* (Freeman, San Francisco, 1975).

[15] L. R. Rabiner and B. Gold, *Theory and Application of Digital Signal Processing* (Prentice-Hall, Englewood Cliffs, NJ, 1975).

[16] P. Grassberger and I. Procaccia, Physica **13D**, 34 (1984).